Title

Dense-Stacking Porous Conjugated Polymer as Reactive-Type Host for High-Performance Lithium Sulfur Batteries

Journal

Angewandte Chemie, 133(20)

ISSN

0044-8249

Authors

Wang, Xiaowei
Yang, Yangyuchen
Lai, Chen
et al.

Publication Date

2021-05-10

DOI

10.1002/ange.202016240

Peer reviewed

Dense-Stacking Porous Conjugated Polymer as Reactive-Type Host for High-Performance Lithium Sulfur Batteries

Xiaowei Wang, Yangyuchen Yang, Chen Lai, Runlai Li, Haomin Xu, Darren H. S. Tan, Kun Zhang, Wei Yu, Oeystein Fjeldberg, Ming Lin, Wei Tang, Ying Shirley Meng,* and Kian Ping Loh**

Abstract: *Commercialization of the lithium-sulfur battery is hampered by bottlenecks like low sulfur loading, high cathode porosity, uncontrollable Li_2S_x deposition and sluggish kinetics of Li_2S activation. Herein, we developed a densely stacked redox-active hexaazatrinaphthylene (HATN) polymer with a surface area of 302 $m^2 g^{-1}$ and a very high bulk density of ca. 1.60 $g cm^{-3}$. Uniquely, HATN polymer has a similar redox potential window to S, which facilitates the binding of Li_2S_x and its transformation chemistry within the bulky polymer host, leading to fast Li_2S/S kinetics. The compact polymer/S electrode presents a high sulfur loading of ca. 15 $mg_s cm^{-2}$ (200-μm thickness) with a low cathode porosity of 41 %. It delivers a high areal capacity of ca. 14 $mAh cm^{-2}$ and good cycling stability (200 cycles) at electrolyte–sulfur (E/S) ratio of 5 $\mu L mg_s^{-1}$. The assembled pouch cell delivers a cell-level high energy density of 303 $Wh kg^{-1}$ and 392 $Wh L^{-1}$.*

Introduction

The rising demand for high energy density and economical energy storage systems for electric vehicles and electric grid has prompted intensive research on alternatives beyond Li-ion batteries. Among the post Li-ion batteries, Li-S battery is deemed one of the most promising energy storage systems due to its sustainability and high energy density.[1,2] However, daunting challenges have to be overcome for the commercialization of Li-S battery owing to a multitude of problems. These include the dissolution of lithium polysulfides, uncontrollable deposition of Li_2S, insulating nature of S/Li_2S, low sulfur loading and excessive electrolyte usage.[3,4] Firstly, polysulfide dissolution leads to low Coulombic efficiency (CE) and capacity fading, and its shuttling effect degrades the lithium anode.[5,6] Secondly, S and Li_2S tend to aggregate during discharge/charge, which causes their poor redistribution and difficult activation,[3,7] resulting in low utilization of active materials. In addition, the preparation of high sulfur loading electrode is hampered by the tendency of electrode cracking in the presence of nanomaterials as S host.[8] Lastly, the use of high surface area host materials consumes a large amount of electrolyte, which limits both the gravimetric and volumetric energy density (E_g and E_v).[9]

Numerous strategies have been devised to address the above challenges, including electrolyte modification,[10] Li metal protection,[11,12] and materials development.[1] To control the polysulfide deposition process, the binding between host materials and the sulfur species must be improved to promote the nucleation and growth of S/Li_2S, rather than random precipitation and agglomeration during discharge/charge that cause inactive S/Li_2S formation.[3,13] Strong polysulfides binding is important to regulate the formation of S/Li_2S. To alleviate polysulfide dissolution, common strategies include adsorption on high surface area host and confinement of nanomaterials[2,14,15] and chemical adsorption by electro-affinity between lithium polysulfide and lithiophilic atoms like N, O, S, and F,[13,16] or transition metal atoms such as V, Co, Mn, Mo, Ti.[15,17–19] However, high-surface-area nanomaterials not only pose difficulty in preparing compact electrode with high sulfur loading, but also result in the consumption of high volume of electrolyte owing to high electrode porosity, ultimately compromising the practical energy density of Li-S batteries. Currently, compact Li-S cathodes based on bulky materials are typically achieved by either calendaring or secondary-granulation techniques,[4] however, the preparation process results in insufficient polysulfide reactive sites, and poor wettability of polysulfide and the electrolyte, leading to capacity fading and damage to lithium anode.[4] Therefore, to address the dilemma, there is urgent need to develop compact electrode with high sulfur loading and low porosity. In terms of developing a bulky electrode material, how do we balance the need for high tap

[*] X. Wang, R. Li, H. Xu, K. Zhang, W. Yu, Prof. Dr. K. P. Loh
Department of Chemistry, National University of Singapore
3 Science Drive 3, 117543 Singapore (Singapore)
E-mail: chmlohkp@nus.edu.sg

D. H. S. Tan, O. Fjeldberg, Prof. Dr. Y. S. Meng
Department of NanoEngineering, University of California San Diego
La Jolla, CA 92093 (USA)
E-mail: shirleymeng@ucsd.edu

C. Lai, Prof. Dr. W. Tang
School of Chemical Engineering and Technology
Xi'an Jiaotong University, Xi'an 710049, Shannxi (China)
E-mail: tangw2018@mail.xjtu.edu.cn

X. Wang
NUS Graduate School for Integrative Sciences and Engineering,
National University of Singapore
21 Lower Kent Ridge Road, 119077 Singapore (Singapore)

Y. Yang, Prof. Dr. Y. S. Meng
Materials Science and Engineering
University of California San Diego, La Jolla, CA 92121 (USA)

H. Xu, Dr. M. Lin
Institute of Materials Research and Engineering, A*STAR
2 Fusionopolis Way, Innovis, 138634 Singapore (Singapore)

Supporting information and the ORCID identification number(s) for the author(s) of this article can be found under:
https://doi.org/10.1002/anie.202016240.

density while enjoying sufficient intrinsic porosity to enable high sulfur loading as well as efficient polysulfide adsorption?

To address the challenges above, we have developed a redox-active porous conjugated polymer (abbreviated as HATN polymer) in this work that has the same redox potential window as sulfur. HATN polymer serves as a Li_2S_x reactive-type host to regulate polysulfide deposition, leading to the uniform deposition of nanostructured Li_2S and S within the bulky porous polymer matrix. Our approach is distinct from common strategies relying on physical or chemical adsorption of polysulfides on high-surface-area materials. Although the surface area of HATN polymer is moderately high (302 $m^2 g^{-1}$), what is important is that it has a very high bulk density of ca. 1.60 $g cm^{-3}$. These attributes enable the preparation of compact electrode with a high sulfur loading of ca. 15 $mg_s cm^{-2}$ and thickness of 200 μm on carbon-coated Al foil, while maintaining a good electrode porosity of 41 % for polymer/S without calendaring. Our polymer/S cathode delivers a high areal capacity of ca. 14 $mAh cm^{-2}$ and good cycling stability of 200 cycles with an Electrolyte-Sulfur (E/S) ratio of 5 $\mu L mg^{-1}$, complying with stringent metric of lean electrolyte in Li-S community. The scalability of HATN polymer and the high areal capacity of polymer/S had been verified by pouch cell test delivering a high energy density of 303 $Wh kg^{-1}$ and 392 $Wh L^{-1}$.

Results and Discussion

The proposed Li_2S_x reactive-type interaction strategy is based on designing redox-active materials that have the same electrochemical window with S redox, and leveraging on site-specific and strong polysulfides binding within the polymer matrix to regulate the formation of S/Li_2S. Organic materials are advantageous due to sustainability, synthetic scalability, and tailorable reactive sites, yet organic materials are typically disadvantaged by low conductivity, low density, and electrode dissolution.[20–22] To overcome these drawbacks, we have selected Hexaazatrinaphthylene (HATN) as the redox-active core since it boasts 6 bidentate N atoms that are able to undergo lithiation/delithiation during discharge-charge, presenting multi-electron redox capability within the S electrochemical window.[20,22] To avoid the formation of low density polymer products prepared with solution-based methods,[23–25] we performed catalyzed melting polymerization by high temperature annealing to prepare densely stacked polymer (Figure 1a; Supporting Information, Figure S1). Details on the synthesis of both the monomer and HATN polymer are provided in the Supplementary. Characterization studies revealed that HATN polymer is bulky and dense compared to nanosheets of the monomer with low bulk density (Supporting Information, Figures S2 and S3). Figure 1b presents the N_2-adsorption isotherms of the polymer and its pore-size distribution plot, wherein the polymer exhibits a good BET of 302.18 $m^2 g^{-1}$ with a main pore-size of 1.11 nm, which is identical with the designed porosity by s-triazine polymerization.

From Figure 1c and d, the 2D layered morphology of HATN polymer is apparent, suggesting that the planar fused conjugated monomer undergoes 2D polymerization. To appreciate the potential of HATN polymer to serve as an electrode with high tap density, we compare its bulk density with that of conventional host materials for sulfur[26,27] at the same mass (Figure 1e). HATN polymer has a bulk density of ca. 1.60 $g cm^{-3}$, which is close to that of graphite. In addition, the porosity and S affinity of HATN[25] polymer render it a good host for sulfur, where sulfur loading up to a weight percentage of 80 % in composite can be achieved by highly efficient melting-infusion (Figure 1f; Supporting Information, Figure S5). HATN polymer also forms a uniform composite with S, as verified from the SEM images with element mapping and by comparing with super P/S composite (Supporting Information, Figure S5). A radar chart is plotted based on parameters such as surface area, conductivity, affordability, stability, bulk density and reactivity with polysulfides (Figure 1g). The plot details are provided in the Supporting Information, Figure S6 and Table S1. From these comparative studies, it is clear that HATN polymer outperforms other host materials. This is underpinned by the high Li ~ Li_2S_x reactivity of HATN polymer originating from its redox-active cores; its optimized surface area with high bulk density affords a compact electrode, which is beneficial in suppressing polysulfide dissolution.

As shown in Figure 2a and the Supporting Information, Video 1, at the incipient stage, both HATN polymer and S undergo lithiation synergistically. The Li_2S_x formed then lithiates the open redox-active bidentate N sites of the polymer, which helps to bind the polysulfides to the polymer matrix strongly. Subsequently, the deposition of Li_2S_x undergoes a regulated chain shortening process. Lithiation/delithiation of the polymer by Li_2S_x and Li_2S_x chain-shortening evolution are discussed below. The cyclic voltammetry curves of HATN and HATN/S electrode in Figure 2b reveal that their individual redox reactions can be distinguished. HATN polymer features two reversible redox couples located at 1.8/2.05 V and 2.4/2.65 V within the sulfur redox potential window, whereas polymer/S exhibits an enhanced sulfur redox behavior with diminishing polarization of anodic and cathodic peaks, suggesting strong interaction between the polymer and sulfur. The electrochemical behavior of HATN polymer/S is distinct from compounds like CuO,[28] VO_2,[28,29] MoO_3,[30] and Mo_6S_8[18] that were previously used as Li_2S_x immobilizers within the sulfur electrochemical window, because these host materials and sulfur show independent redox behaviors in their CV curves. Further investigation of the Li_2S_x-reactive type process is needed to understand the role of HATN polymer. Here we used an electrolyte of 1 M Li_2S_6 in dioxolane/dimethoxyethane (DOL/DME) as the sole Li^+ source to study the discharge/charge behaviour of the polymer, which is shown in Figure 2c. First, HATN polymer has a specific capacity of 700 $mAh g_{polymer}^{-1}$ at the first discharge, which is much higher than the capacity of super P (400 $mAh g_{super\ P}^{-1}$; Supporting Information, Figure S7a). This indicates the efficient deposition of Li_2S_x onto the polymer matrix to form Li_2S. Secondly, the first charge delivers a matching capacity with the plateau capacity during the first discharge in the profile, suggesting that the as-formed Li_2S in the polymer can be completely oxidized into Li_2S_x, and only

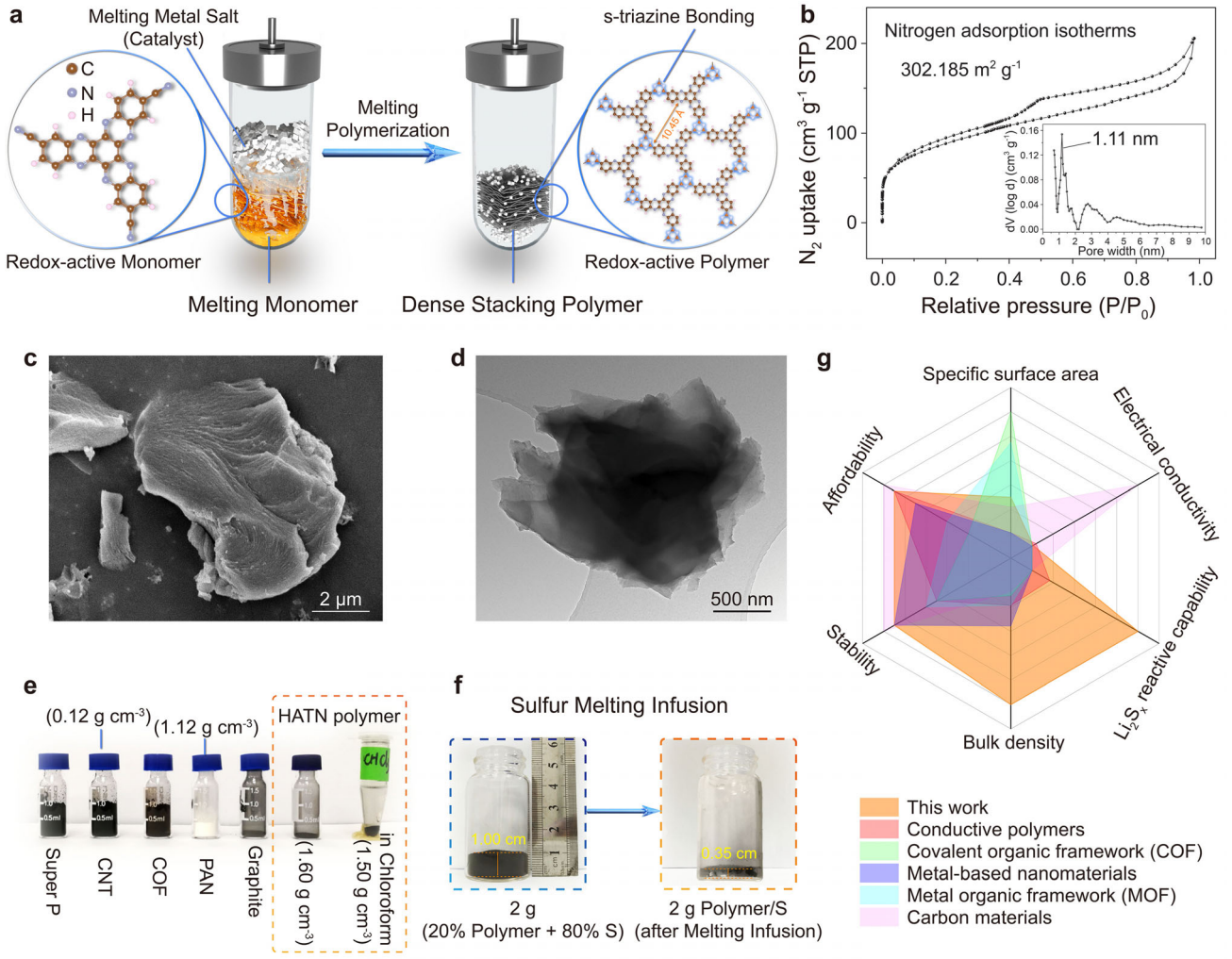

Figure 1. Characterizations of polymer and polymer/sulfur composite and the comparison of various types of sulfur host materials. The polymer synthesis from the monomer (a), N_2 adsorption isotherms and pore-size distribution plots of the polymer (b), SEM and TEM images of the bulky polymer (c, d), the comparison of bulk density of materials at 50 mg (e), the schematic illustration of sufficient sulfur infusion into the dense porous polymer (cooled down after 155 °C for 12 h, f), and the radar chart of various factors for the guidance and evaluation of S host materials (g).

these strongly bound Li_2S_x continue to be oxidized into S excluding outer Li_2S_6 from oxidizing in the polymer. Compared to super P, the polymer presents longer discharge plateaus with high CE (Supporting Information, Figure S7a), which indicates the effective suppression of polysulfides owing to the strong binding of Li_2S_x to the redox-active polymer. Furthermore, HATN polymer shows declining voltage overshoot related to easier Li_2S activation (Figure 2c, inset) suggesting good reaction kinetics. Moreover, the lithiation reaction of the polymer by Li_2S_x is verified from the evolution of the different chemical states in the N1s XPS signals (Figure 2d) corresponding to the different discharge states in Figure 2c. The XPS signal of C=N at 399.02 eV[25] vanishes along with the formation of C–N at 400.02 eV[23] owing to polymer lithiation, and the C=N peak restores after delithiation. The presence of nitrogen oxide derivatives indicates a solvent decomposition-derived solid-electrolyte-interface (SEI) on the polymer.[31] In the meantime, the FTIR spectra of the polymer in the polymer-Li_2S_6 test (Supporting Information, Figure S7b), at pristine state, 100% depth-of-discharge (DOD) and depth-of-charge (DOC) states confirm both the opening and restoration of bidentate C=N during lithiation/delithiation. In Figure 2e and the Supporting Information, Figure S7c–e, we further investigated polysulfide interactions with various host materials, including carbon (physical adsorption), polymer (chemical adsorption), and lithiated-polymer (reactive-type binding). When Li atom of Li_2S_x binds to polymer N, the binding energy of Li1s peak of -C=N $(\delta^-)\cdots(\delta^+)$ Li-S_x in polymer/Li_2S_x is shifted to higher binding energy of 56.2 eV (higher oxidation state). The Li1s peak of the lithiated-polymer (-C–N–Li) is located at 55.2 eV; upon binding of Li_2S_x to the lithiated-polymer, the peak shifts to higher binding energy. The presence of chemically-shifted peaks in the XPS spectra indicates that polysulfide binds with the lithtiated-polymer forming stable structures (C–N–Li–S_x), in agreement with the DFT results shown in Figure 3c.

In-situ X-ray diffraction (XRD) investigation of polymer/S electrode during discharge/charge was conducted to explore

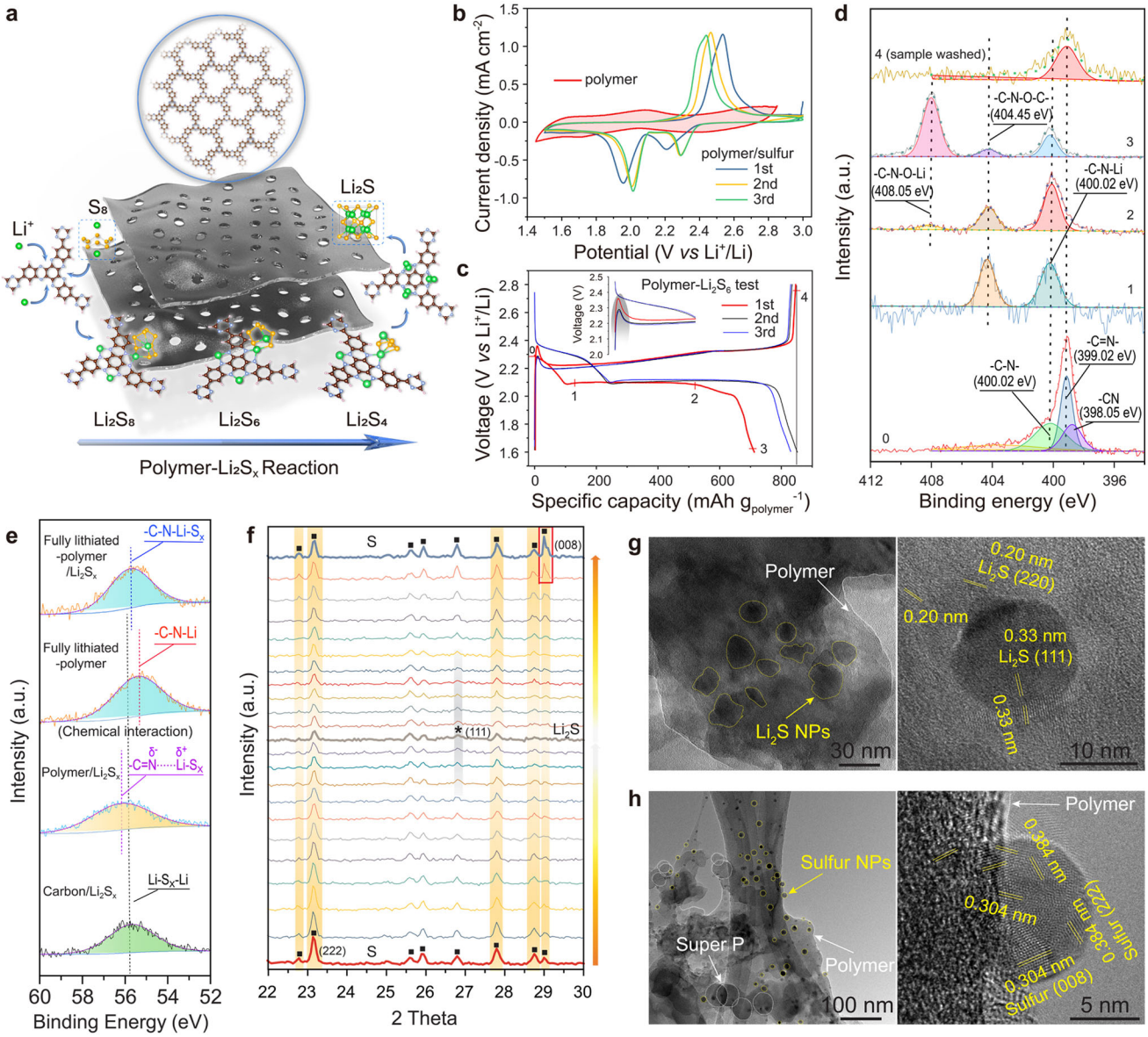

Figure 2. Characterizations of Li_2S_x-reactive pathway and the growth of Li_2S/S during discharge/charge. The Li_2S_x-reactive pathway (a), CV curves of the polymer and polymer/S electrode (b), Voltage profiles of polymer-Li_2S_6 test and the correlated N1s XPS spectra (c, d), the Li1s XPS spectra of various host materials of carbon, polymer, and lithiated-polymer with Li_2S_x interactions (e), In-situ XRD patterns of thick HATN polymer/S electrode (f), and HRTEM images characterized at 200 kV, showing the morphology and nano-crystallinity of the electrochemically-formed Li_2S/S (g and h).

the nucleation and growth process of Li_2S/S. The Supporting Information, Figure S8a shows the discharge/charge profile of polymer/S electrode at 0.35 mA cm^{-2} with the correlated 2D-view XRD patterns, which monitors the real-time reversible transformation between S and Li_2S in the electrode (see experimental details in the Supporting Information). Figure 2f plots the XRD patterns recorded for the different electrode states to track the corresponding species. Specifically, the intensity of the characteristic peaks of sulfur at 23.1°, 25.9°, 27.9°, 28.8°, and 29.0°[10,32] decline and intensify in sequence with discharge/charge. The crystal face orientation of S (008) peak at 29.0° is observed in Figure 2f and Figure S8a, indicating the redistribution of sulfur with self-optimized crystallinity (Figure 2h). The peak at 26.8° that appears after discharge is attributed to the (111) crystal plane of Li_2S, which is also confirmed by high-resolution-transmission-electron-microscopy (HRTEM) images in Figure 2g. Moreover, it is shown that nanostructured Li_2S and S are anchored within the porous polymer matrix (Figure 2g and Figure 2h; Supporting Information, Figure S8b–d). This effectively improves the reaction kinetics (Figure 2c, inset) by excluding the formation of a thick insulating layer of Li_2S/S.[3] Thus, the Li_2S_x reactive-type polymer host offers a strategy to improve the electrochemical kinetics of Li_2S/S nanomaterials, which is of great interests currently in the Li-S battery community.[33–36] The nanostructured Li_2S and S mixed in the

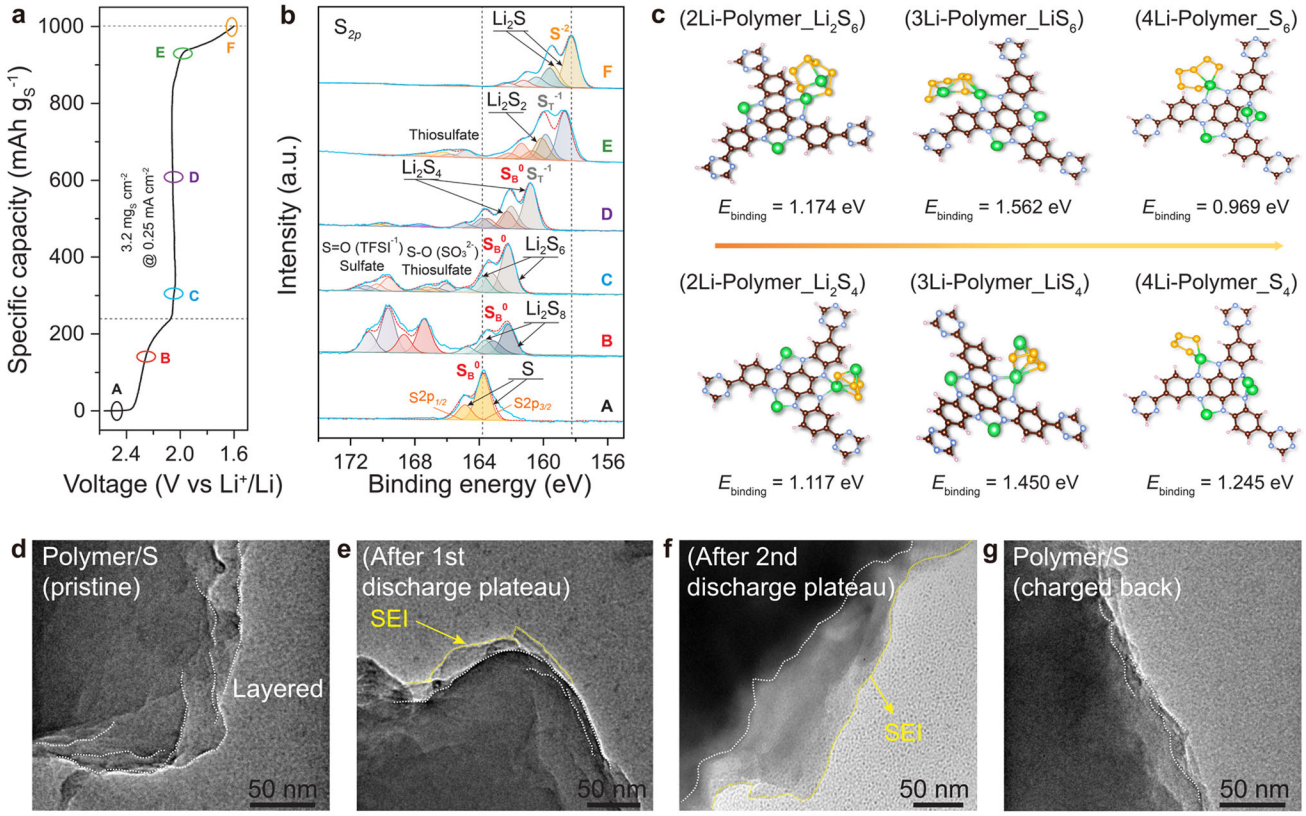

Figure 3. Investigation of the interaction of the polymer with Li_2S_x during discharge showing a controllable deposition process. The ex-situ (Argon-protected condition) S_{2p} X-ray photoelectron spectroscopy (XPS) analysis of polymer/S electrode, extracted from cells at different discharge states (a, b), DFT calculation results of Li_2S_x binding to the initially lithiated polymer (c), and the evolution of SEI on the polymer during the first cycle (d–g).

polymer matrix could be directly visualized by HRTEM, unlike the bulky or electron-beam vulnerable counterpart.[35,37] (Supporting Information, Figure S9a,b). Furthermore, the nucleation and growth of nanostructured Li_2S/S in polymer/S electrode reconcile with the results in the polymer-Li_2S_6 test above (Supporting Information, Figure S9c,d), confirming that the polymer-Li_2S_x reaction drives the transformation of polysulfides into nanostructured Li_2S and S.

The interaction of the polymer with lithium polysulfides was tracked by monitoring the chemical states of S 2*p* using X-ray photoelectron spectroscopy (XPS) analysis at different discharge states (argon-protected condition), as shown in Figure 3 a and b. From the galvanostatic plot, HATN polymer/S electrode has two discharge plateaus located at 2.3 V and 2.08 V that corresponded to S lithiation and the transformation from Li_2S_x into Li_2S, respectively. It features an extended second discharge plateau with a capacity ratio of 1:3 close to the theoretical transformation of S to Li_2S,[1,38] which is superior to most reports ($<$1:2.5).[3,10,17] A control sample of super P/S, prepared with the same melting-infusion method and sulfur loading, only achieved a capacity ratio of 1:2.2 at the same current density (Supporting Information, Figure S10a). Figure 3 b shows the characteristic peaks of S (164.1 eV, $S2p_{3/2}$), Li_2S (159.6 eV, $S2p_{3/2}$),[17,36] and Li_2S_x (referring to Li_2S_4, 1:1 ratio of the two $S2p_{3/2}$ contributions at 160.8 eV, $S_{Terminal}^{-1}$ and 162.1 eV, $S_{Bridging}^{0}$)[17] for polymer/S electrode. It presents a stepwise evolution of S_{2p} XPS from S_B to S_T that accompanies the ring opening and chain shortening of Li_2S_x during discharge,[38] illustrating a controllable Li_2S_x deposition process compared to super P with weak Li_2S_x-interaction (Supporting Information, Figure S10b). The strong S_B signal suggests that long chain Li_2S_8 and Li_2S_6 produced after 1st discharge plateau could be stabilized in ring geometry, which is consistent with the density-functional-theory (DFT) calculation results of Li_2S_x (x = 8, 6 and 4) binding to the polymer in Figure 3 c (details in the Supporting Information, Table S2). Specifically, Li_2S_x with longer chains has stronger binding in the favorable ring geometry with the polymer, evident from the decreasing $E_{binding}$ of Li_2S_8, Li_2S_6, and Li_2S_4 (1.276, 1.174, 1.117 eV). Furthermore, Li_2S_x offers Li^+ to lithitate the vacant bidentate N atoms of polymer and the detached LiS_x (x = 6 and 4) binds the lithiated polymer by structure optimization, presenting higher $E_{binding}$ of LiS_6 and LiS_4 compared to Li_2S_6 and Li_2S_4 (1.562 vs. 1.174 eV, 1.450 vs. 1.117 eV). Furthermore, the reaction between the polymer and Li_2S_x is traced by looking at changes in the thin layer morphology arising from the formation and deformation of SEI on the polymer, which is consistent with that on HATN-based electrodes for Li ion batteries[20,23] (seen from the TEM images in Figure 3 d–g). Therefore, we can conclude that the

N-rich redox-active sites in HATN polymer promote strong binding with polysulfides, which is conducive to controlling the deposition of S/Li_2S during discharge/charge.[3,4]

It is challenging to achieve a practical high energy density Li-S full cell as it has to make the trade-off between high capacity and low electrolyte usage.[9,26,39] In this scenario, the electrochemical performance of polymer/S electrode is evaluated with a stringent E/S ratio of 5 $\mu L\,mg_S^{-1}$ in a typical Li-S electrolyte.[39] Figure 4a shows the galvanostatic intermittent titration test (GITT) studies of polymer/S and super P/S with similar sulfur loadings to reveal the kinetic and thermodynamic advantages of using HATN polymer over super P. Both GITT profiles reveal characteristic discharge-charge curves of Li-S battery, but polymer/S electrode features more stable and higher plateau capacities with minor polarization, which indicates better reaction kinetics. Besides, the deviation between the practical voltages at constant current pulse and the equilibrium voltages (dotted curve) at steady state (open-circuit-voltage, OCV) as a function of the state of discharge and charge, reflects the chemical diffusion coefficient of the electrode during relaxation process (OCV).[10] The voltage of polymer/S generally relaxes faster to the equilibrium (much smaller voltage deviation) during the discharge process, which suggests a high diffusion coefficient and a high concentration of polysulfides attached to the electrode through much stronger binding to the polymer.[10] The redox-active nature of HATN helps mitigate self-discharge after discharge and charge, thus affording stable OCV (Supporting Information, Figure S11a,b). HATN polymer shows comparable adsorption capability for polysulfide as Ketjen black (KB) at pristine state. Although the specific surface area of HATN polymer is much smaller than that of KB (KB-EC-300J, 800 $m^2\,g^{-1}$), its N-rich polymer matrix is highly lithiophilic and attracts lithium polysulfides (Supporting Information, Figure S11c). Figure 4b illustrates the voltage versus areal capacity profiles of polymer/S electrode with super high sulfur loading of 15.4 $mg_s\,cm^{-2}$ (on Al foil by normal slurry-coating) at different current densities; the areal capacity is a useful metric for comparison in the battery industry.[39] The electrode delivers superior areal capacity ranging from 14 to 7.2 $mAh\,cm^{-2}$ with long and flat discharge plateaus, and low overpotential at the current densities from 0.25 to 5 $mA\,cm^{-2}$. The contribution to the overall capacity by the polymer can be obtained based on its mass loading and the specific capacity of ca. 220 $mAh\,g^{-1}$ (Supporting Information, Figure S6c). For a 15 $mg_{sulfur}\,cm^{-2}$ cathode that delivers an areal capacity of 14 $mAh\,cm^{-2}$ (Figure 4b), 3.75 $mg_{polymer}\,cm^{-2}$ (S to polymer mass ratio = 4:1) delivers areal capacity of 0.825 $mAh\,cm^{-2}$. Thus, the contribution by the polymer to the overall capacity is ca. 6%. The actual contribution is less than 6%, since our HATN polymer and sulfur undergo discharge and charge in a concerted fashion in Li-S batteries. Hence, the bulky HATN polymer serves as a Li_2S_x reactive-type host to regulate polysulfide deposition, facilitating the crystal growth of nanostructured Li_2S and S. The high-areal-capacity performance hits the highest benchmark under lean electrolyte condition on carbon-coated Al current collector,[4,29,40] which shows great promise for practical high energy density Li-S battery. The superior capacity is attributed to the compact electrode enabled by the bulky and dense polymer host, making most use of the electrolyte. This is also evident from the GITT performance of the polymer/S electrode at the relevant current densities (Supporting Information, Figure S11d), delivering areal capacities similar to those in Figure 4b.

Our polymer/S electrode displays excellent rate capability (Figure 4c), achieving 14.0, 11.2, 10.1, 9, 8.4, and 7.2 $mAh\,cm^{-2}$ at current densities of 0.25, 0.5, 1, 2, 2.5, and 5 $mA\,cm^{-2}$, respectively. Besides the good reaction kinetics of the polymer/S electrode (Figure 4a; Supporting Information, Figure S12a,b), the strong binding derived from polymer-Li_2S_x reaction, the compactness of the electrode and its good electrical conductivity are instrumental.[18] EIS results (Supporting Information, Figure S13) verify that nanostructured Li_2S and S mediates fast charge-transfer kinetics at the interface of bulky HATN host and electrolyte (GITT of Figure 4a). Additionally, the good electrical conductivity of polymer/S electrodes is validated from the linear relationship between areal capacity and sulfur loading in Figure 4d (well-defined plateaus with similar overpotentials; Supporting Information, Figure S12c), showing high and stable sulfur utilization. HATN polymer provides highly robust electron conduction pathways from the reaction sites of nanostructured Li_2S/S to the current collector (Supporting Information, Figure S13d), because S-Li_2S-S volume change is accommodated by the stable bulky host (Supporting Information, Figure S6d), which avoids losing inter-particle contact. Figure 4e exhibits its excellent long-term cycling stability in a high initial capacity of 10.5 $mAh\,cm^{-2}$ with 80% capacity retention over 200 cycles and high CE, which results from the Li_2S_x-reactive type binding to the polymer, and the efficient utilization of lean electrolyte by the compact polymer/S electrode (compared to excessive electrolyte condition; Supporting Information, Figure S14). The electrochemical performance attained here meets the metrics of lean-electrolyte defined by the Li-S community.[18,39] By comparison with other advanced host materials under stringent lean electrolyte (Supporting Information, Table S3), our HATN polymer/S cathode shows very high sulfur loading and superior areal capacity, which are desirable attributes for addressing the bottleneck of high-capacity cathode for high energy density Li-S batteries.

The electrode evolution after discharge/charge was investigated with regards to the electrode integrity,[8,40] porosity,[18,26] and the redistribution and loss of Li_2S/S for polymer/S cathode,[3] together with the Li anode stability[41] and practical depletion of Li metal in coin-cell. The latter provides the Negative-to-Positive (N/P) capacity ratio, which is useful for guiding pouch-cell assembly.[43] Figure 5a to c display the cross-section SEM images of the thick polymer/S cathodes (with the same sulfur loading of 15.4 $mg_s\,cm^{-2}$ under the same assembly pressure, see the Supporting Information) after first discharge/charge at 1 $mA\,cm^{-2}$, wherein the electrode thickness changes from the pristine 200 μm to 220/187 μm of the discharged/charged (from coin-cell disassembly). HATN polymer/S achieves a high tap density of 1.22 $g\,cm^{-3}$ (Supporting Information, Figure S15a,b), and the associated porosity is 41% for the pristine, 35% for polymer/Li_2S

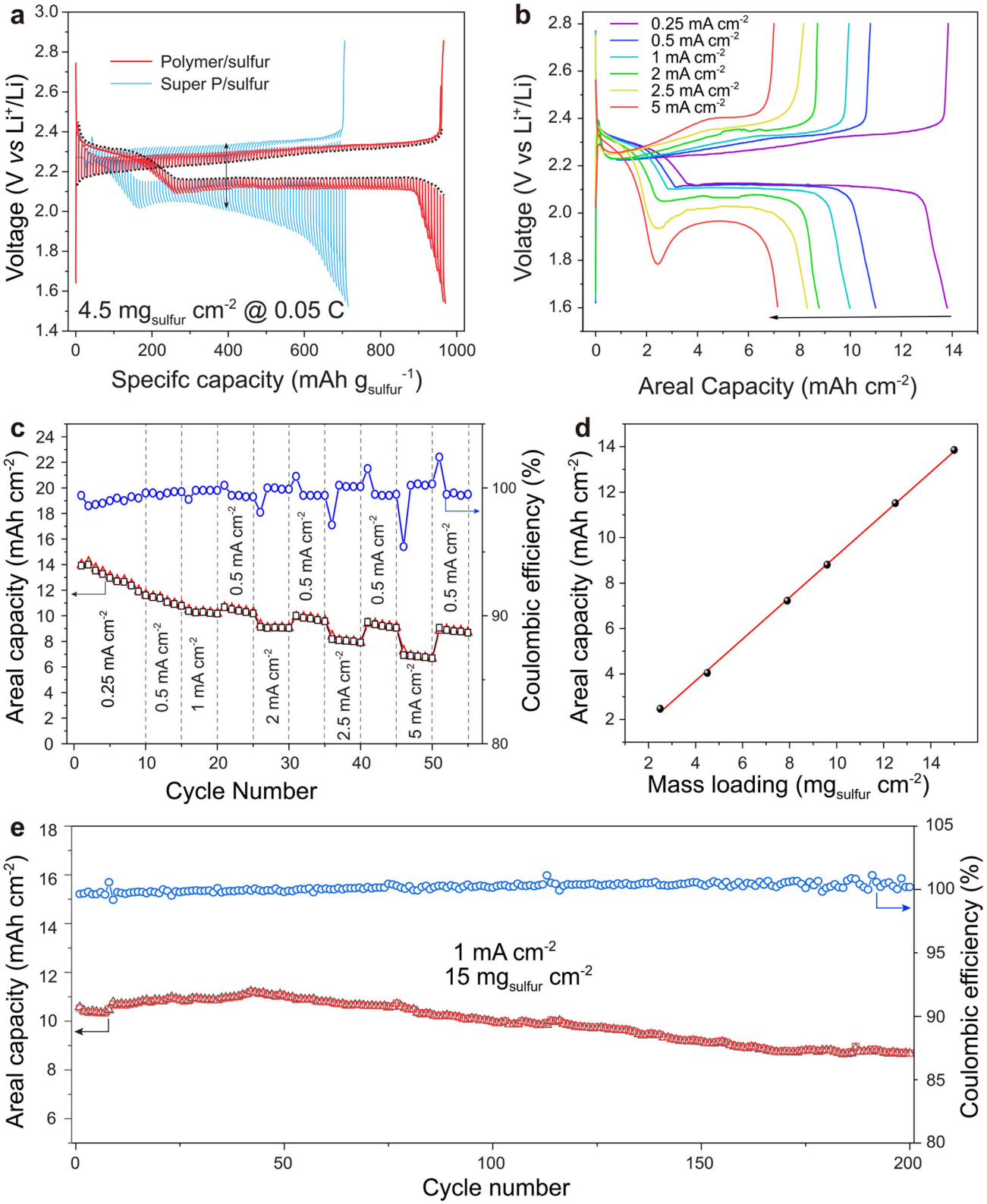

Figure 4. Li-S battery performance. The comparison of GITT performance (a), Discharge/charge profiles of polymer/S electrodes with ca. 15 mg cm^{-2} S loading, and the rate capability (b, c), The plot of areal capacity versus S loading (d), and the long-term cycling stability of polymer/S electrode at 1 mA cm^{-2} with Electrolyte/sulfur E/S ratio of 5 µL mg^{-1} (e).

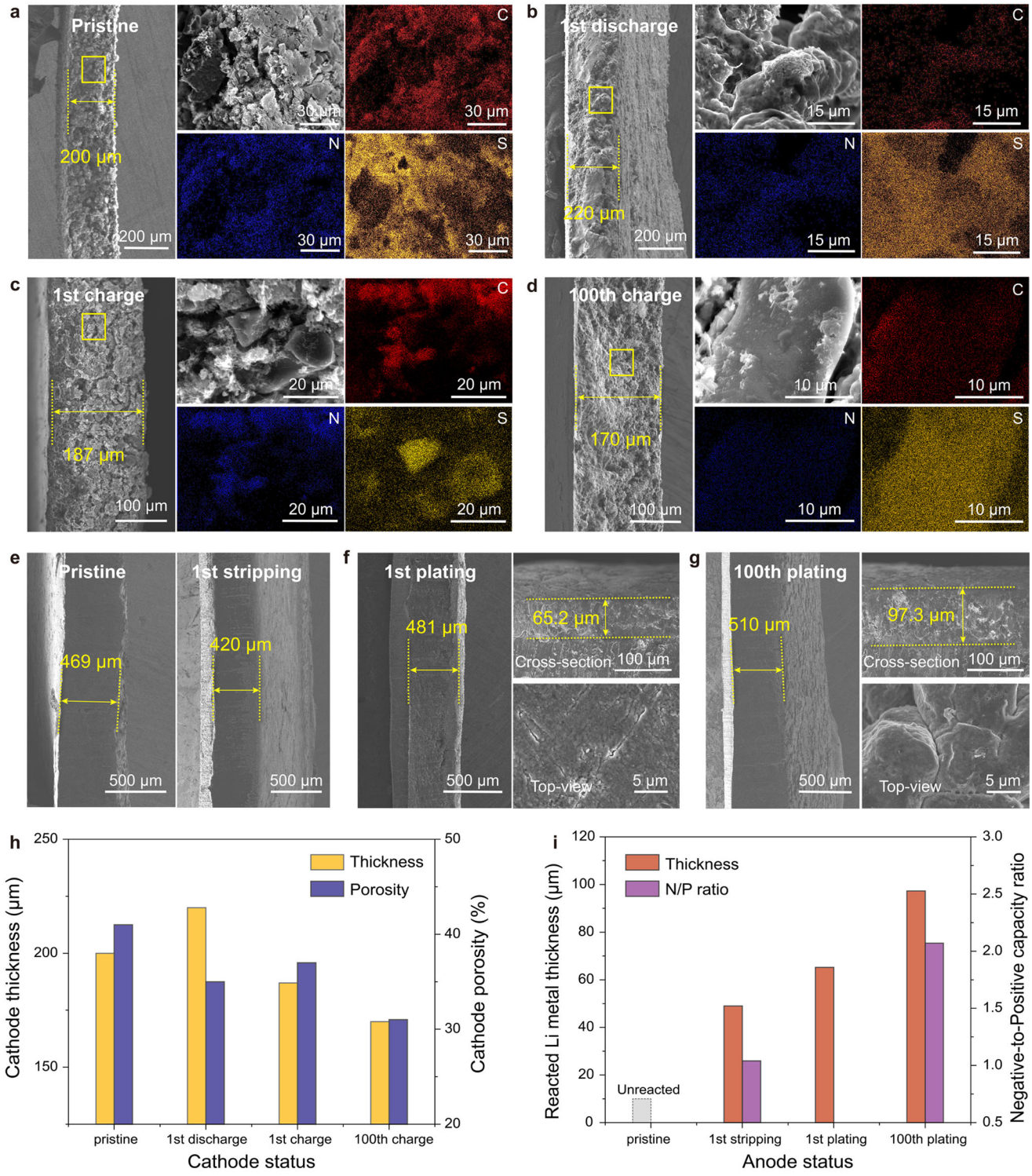

Figure 5. Investigation of the structural change of HATN polymer/S cathode and Li metal anode. Electrode thickness change of polymer/S cathode with 15 $mg_s cm^{-2}$ delivering 10.5 $mAh cm^{-2}$ at 1 $mA cm^{-2}$ during the first cycle from pristine to 1st charge back (a to c) and after 100th charge back (d), Li metal anode from pristine to 1st stripping (e) and after 1st and 100th plating back (f and g), cathode porosity evolution (h) and change in Li anode utilization change (i).

(minor volume change of 10 %) and 37 % for polymer/S after first discharge and charge, respectively, assessed based on the practical electrode volume and dense electrode volume (Supporting Information, Table S4).[26]

The well-maintained porosity after discharge/charge (35 %/37 %) clearly suggests the robustness of the HATN polymer/S electrode against electrode cracking or delamination[8] (see cross-section SEM images from Figure 5a to c).

This is also evident from the uniform Li_2S/S redistribution in the zoomed-in SEM images. Upon further cycling over 100 cycles, polymer/S cathode gets denser with a thickness of 170 µm and a porosity low to 31 % (Figure 5 d). All these results demonstrate that the compact electrode can sustain the volume change during cycling very well due to the bulky and dense polymer host. Figure 5 e–g show the SEM images of the corresponding Li metal paired with the cathodes in Figure 5 a–d in cross-section and top views. After the first discharge relating to Li stripping, a depletion thickness of 49 µm is observed in Figure 5 e, which delivers a theoretical areal capacity of 10.78 mAh cm^{-2},[41] corresponding to positive capacity of 10.5 mAh cm^{-2} (N/P = 1.04). Figure 5 f and g display relatively dense Li plating of 65.2 µm after 1st charge, and 97.3 µm reacted Li layer after 100th charge (low N/P ratio of 21.40/10.3 = 2.07). The efficient utilization of Li anode in coin-cell test was verified from high CE over cycling (Supporting Information, Figure S15d). These results are summarized in Figure 5 h and i.

To validate the scalability of HATN polymer and the high areal capacity of the polymer/S electrode, a practical Li-S pouch cell was assembled. Figure 6 a shows the 5Ah-pouch-cell design in this work, where double-side coated polymer/S cathode, 200 µm Li anode with N/P ratio of 2.00 and lean electrolyte with Electrolyte-Capacity E/C ratio of 3 g Ah^{-1} were used. Detailed parameters are listed in Table S5. The optical images of the as-assembled pouch-cell in Figure 6 b exhibit a cell volume of 0.027 L (length × width × thickness) by actual measurement (the whole process of pouch-cell preparation is provided in Figure S16). The pouch-cell delivers a capacity of 4.92 Ah at 0.02 C with an average working voltage of 2.15 V and 4.15 Ah is retained with small polarization when the current density rises up to 0.1 C (1 C = 5 Ah, Figure 6 c). Consequently, it brings about high energy density of 303 Wh kg^{-1} and 392 Wh L^{-1} by actual measurement. Notably, the long discharge plateaus with high reversibility from the voltage profiles are consistent with the electrochemical performance in coin-cell test (Figure 4).[4,39] The pouch-cell presents superior cycling stability with 78 % capacity retention over 30 cycles, even with such a low E/C ratio (Figure 6 d). Figure 6 e demonstrates that a drone could be powered by two Li-S pouch-cells in tandem to match the rated voltage, reflecting the good energy density together with good rate capability (Figure 6 c and Supplementary video 2). From the comparison of energy density among various energy storage systems in Figure 6 f, our Li-S full-cell reaches high level performance among Li-S studies.[9,18,40,42,43]

Conclusion

We report the synthesis and application of a bulky and dense redox-active porous conjugated HATN polymer as cathode in Li-S battery. It serves as a Li_2S_x reactive-type host to regulate polysulfide electrochemistry, facilitating its transformation into nanostructured Li_2S and S within the porous

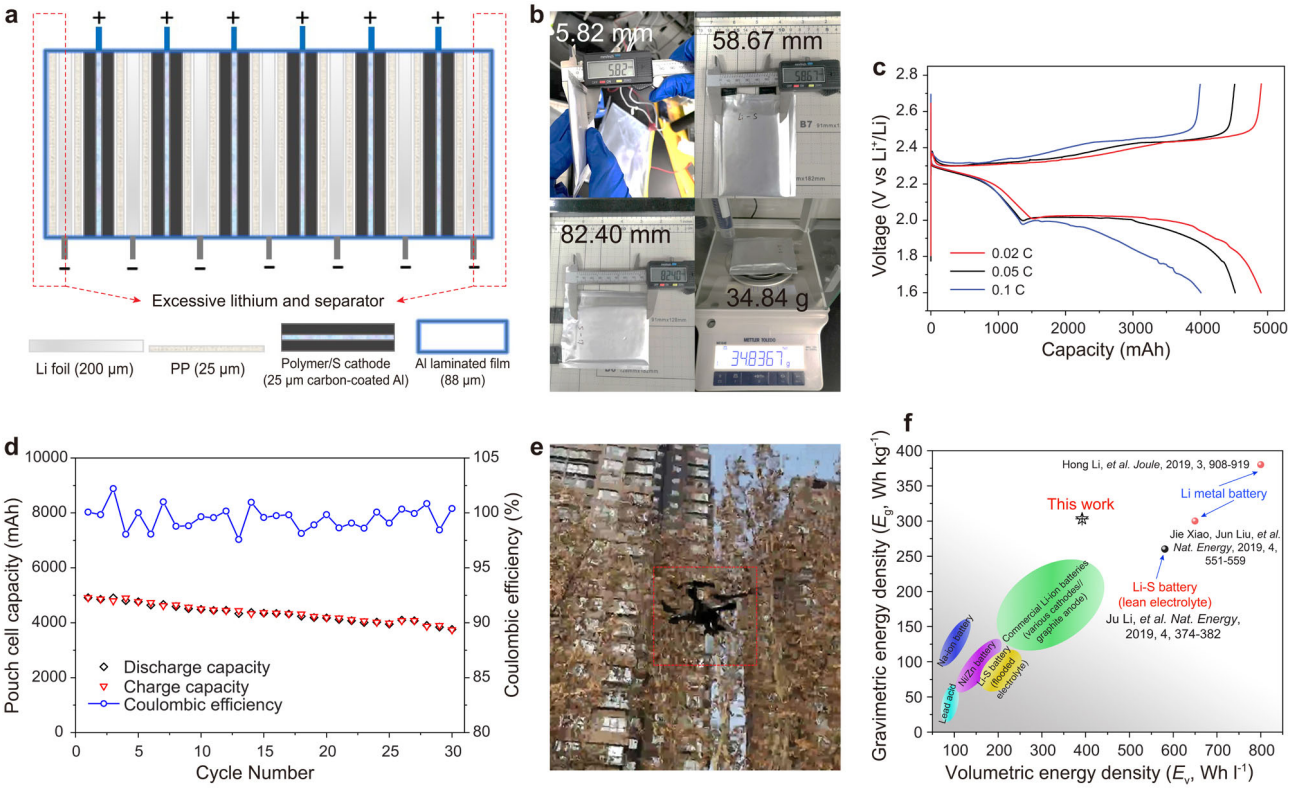

Figure 6. Practical Li-S pouch cell performance evaluation and analysis. The pouch-cell structure and the optical images of the measurement of the assembled pouch-cell (a, b), The voltage profiles of the pouch-cell at various current densities and the cycling behavior (c, d), The optical image of a drone powered by the pouch-cells (e), and energy density comparison among different energy storage systems (f).

polymer matrix. HATN polymer boasts a good surface area of 302 $m^2 g^{-1}$ with a very high bulk density of ca. 1.60 $g cm^{-3}$, which enables compact electrode (200 μm) preparation with high sulfur loading of ca. 15 $mg_s cm^{-2}$ on carbon-coated Al foil, and a low porosity of 41 % without extra-calendaring. As a result, HATN polymer/S cathode delivers a high areal capacity of 14 $mAh cm^{-2}$, and excellent capacity retention of 80 % (initially 10.5 $mAh cm^{-2}$) over 200 cycles, along with high CE and low E/S ratio of 5 $\mu L mg^{-1}$. Further, the scalability of our polymer and the high areal capacity of polymer/S electrode had been verified by the pouch cell test, where a cell-level high energy density of 303 $Wh kg^{-1}$ (392 $Wh L^{-1}$), and good cycling stability of 30 cycles with a low E/C ratio of 3 $g Ah^{-1}$ were attained. Our study validates that the Li_2S_x-reactive type strategy is effective in regulating the growth of nanostructured Li_2S/S, contributing to the optimal design of Li-S battery.

Acknowledgements

K.P.L. acknowledges NRF-CRP grant "Two-Dimensional Covalent Organic Framework: Synthesis and Applications", grant number NRF-CRP16-2015-02, funded by National Research Foundation, Prime Minister's Office, Singapore. W.T. acknowledges support from the National Natural Science Foundation of China (Grant No. 21905220 and 21503158). Y.S.M. acknowledges funding support from Zable Endowed Chair of Energy Technology and the Sustainable Power & Energy Center of UC San Diego.

Conflict of interest

The authors declare no conflict of interest.

Keywords: bulky host · dense stacking · high areal capacity · high practical energy density · redox-induced polysulfide deposition

[1] P. G. Bruce, S. A. Freunberger, L. J. Hardwick, J. M. Tarascon, *Nat. Mater.* **2012**, *11*, 19 – 29.
[2] X. Ji, K. T. Lee, L. F. Nazar, *Nat. Mater.* **2009**, *8*, 500 – 506.
[3] H. Pan, J. Chen, R. Cao, V. Murugesan, N. N. Rajput, K. S. Han, K. Persson, L. Estevez, M. H. Engelhard, J.-G. Zhang, K. T. Mueller, Y. Cui, Y. Shao, J. Liu, *Nat. Energy* **2017**, *2*, 813 – 820.
[4] Q. Pang, X. Liang, C. Y. Kwok, J. Kulisch, L. F. Nazar, *Adv. Energy Mater.* **2017**, *7*, 1601630.
[5] W. Li, H. Yao, K. Yan, G. Zheng, Z. Liang, Y. M. Chiang, Y. Cui, *Nat. Commun.* **2015**, *6*, 7436 – 7443.
[6] S. S. Zhang, *J. Power Sources* **2016**, *322*, 99 – 105.
[7] L. Kong, Q. Jin, J. Q. Huang, L. D. Zhao, P. Li, B. Q. Li, H. J. Peng, X. Zhang, Q. Zhang, *Energy Technol.* **2019**, *7*, 1900111.
[8] D. Lv, J. Zheng, Q. Li, X. Xie, S. Ferrara, Z. Nie, L. B. Mehdi, N. D. Browning, J.-G. Zhang, G. L. Graff, J. Liu, J. Xiao, *Adv. Energy Mater.* **2015**, *5*, 1402290.
[9] C. Weller, S. Thieme, P. Härtel, H. Althues, S. Kaskel, *J. Electrochem. Soc.* **2017**, *164*, A3766 – A3771.
[10] Q. Pang, A. Shyamsunder, B. Narayanan, C. Y. Kwok, L. A. Curtiss, L. F. Nazar, *Nat. Energy* **2018**, *3*, 783 – 791.
[11] N. Li, Q. Ye, K. Zhang, H. Yan, C. Shen, B. Wei, K. Xie, *Angew. Chem. Int. Ed.* **2019**, *58*, 18246 – 18251; *Angew. Chem.* **2019**, *131*, 18414 – 18419.
[12] Y. X. Ren, L. Zeng, H. R. Jiang, W. Q. Ruan, Q. Chen, T. S. Zhao, *Nat. Commun.* **2019**, *10*, 3249 – 3258.
[13] G. Li, X. Wang, M. H. Seo, M. Li, L. Ma, Y. Yuan, T. Wu, A. Yu, S. Wang, J. Lu, Z. Chen, *Nat. Commun.* **2018**, *9*, 705 – 714.
[14] S. Bai, X. Liu, K. Zhu, S. Wu, H. Zhou, *Nat. Energy* **2016**, *1*, 16094.
[15] W. Tang, Z. Chen, B. Tian, H. W. Lee, X. Zhao, X. Fan, Y. Fan, K. Leng, C. Peng, M. H. Kim, M. Li, M. Lin, J. Su, J. Chen, H. Y. Jeong, X. Yin, Q. Zhang, W. Zhou, K. P. Loh, G. W. Zheng, *J. Am. Chem. Soc.* **2017**, *139*, 10133 – 10141.
[16] J. Song, M. L. Gordin, T. Xu, S. Chen, Z. Yu, H. Sohn, J. Lu, Y. Ren, Y. Duan, D. Wang, *Angew. Chem. Int. Ed.* **2015**, *54*, 4325 – 4329; *Angew. Chem.* **2015**, *127*, 4399 – 4403.
[17] X. Liang, C. Hart, Q. Pang, A. Garsuch, T. Weiss, L. F. Nazar, *Nat. Commun.* **2015**, *6*, 5682 – 5689.
[18] W. Xue, Z. Shi, L. Suo, C. Wang, Z. Wang, H. Wang, K. P. So, A. Maurano, D. Yu, Y. Chen, L. Qie, Z. Zhu, G. Xu, J. Kong, J. Li, *Nat. Energy* **2019**, *4*, 374 – 382.
[19] X. Liu, J. Q. Huang, Q. Zhang, L. Mai, *Adv. Mater.* **2017**, *29*, 1601759.
[20] C. Peng, G.-H. Ning, J. Su, G. Zhong, W. Tang, B. Tian, C. Su, D. Yu, L. Zu, J. Yang, M.-F. Ng, Y.-S. Hu, Y. Yang, M. Armand, K. P. Loh, *Nat. Energy* **2017**, *2*, 17074 – 17082.
[21] M. Armand, S. Grugeon, H. Vezin, S. Laruelle, P. Ribiere, P. Poizot, J. M. Tarascon, *Nat. Mater.* **2009**, *8*, 120 – 125.
[22] Y. Hanyu, T. Sugimoto, Y. Ganbe, A. Masuda, I. Honma, *J. Electrochem. Soc.* **2014**, *161*, A6 – A9.
[23] M. Mao, C. Luo, T. P. Pollard, S. Hou, T. Gao, X. Fan, C. Cui, J. Yue, Y. Tong, G. Yang, T. Deng, M. Zhang, J. Ma, L. Suo, O. Borodin, C. Wang, *Angew. Chem. Int. Ed.* **2019**, *58*, 17820 – 17826; *Angew. Chem.* **2019**, *131*, 17984 – 17990.
[24] J. Wang, C. S. Chen, Y. Zhang, *ACS Sustainable Chem. Eng.* **2018**, *6*, 1772 – 1779.
[25] S. N. Talapaneni, T. H. Hwang, S. H. Je, O. Buyukcakir, J. W. Choi, A. Coskun, *Angew. Chem. Int. Ed.* **2016**, *55*, 3106 – 3111; *Angew. Chem.* **2016**, *128*, 3158 – 3163.
[26] N. Kang, Y. Lin, L. Yang, D. Lu, J. Xiao, Y. Qi, M. Cai, *Nat. Commun.* **2019**, *10*, 4597 – 4606.
[27] Q. Pang, C. Y. Kwok, D. Kundu, X. Liang, L. F. Nazar, *Joule* **2019**, *3*, 136 – 148.
[28] X. Liang, C. Y. Kwok, F. Lodi-Marzano, Q. Pang, M. Cuisinier, H. Huang, C. J. Hart, D. Houtarde, K. Kaup, H. Sommer, T. Brezesinski, J. Janek, L. F. Nazar, *Adv. Energy Mater.* **2016**, *6*, 1501636.
[29] Y. Song, W. Zhao, L. Kong, L. Zhang, X. Zhu, Y. Shao, F. Ding, Q. Zhang, J. Sun, Z. Liu, *Energy Environ. Sci.* **2018**, *11*, 2620 – 2630.
[30] L. Luo, X. Qin, J. Wu, G. Liang, Q. Li, M. Liu, F. Kang, G. Chen, B. Li, *J. Mater. Chem. A* **2018**, *6*, 8612 – 8619.
[31] X.-B. Cheng, C. Yan, X. Chen, C. Guan, J.-Q. Huang, H.-J. Peng, R. Zhang, S.-T. Yang, Q. Zhang, *Chem* **2017**, *2*, 258 – 270.
[32] J. Conder, R. Bouchet, S. Trabesinger, C. Marino, L. Gubler, C. Villevieille, *Nat. Energy* **2017**, *2*, 17069 – 17075.
[33] S.-K. Lee, Y. J. Lee, Y.-K. Sun, *J. Power Sources* **2016**, *323*, 174 – 188.
[34] H. Yan, H. Wang, D. Wang, X. Li, Z. Gong, Y. Yang, *Nano Lett.* **2019**, *19*, 3280 – 3287.
[35] Z.-L. Xu, S. J. Kim, D. Chang, K.-Y. Park, K. S. Dae, K. P. Dao, J. M. Yuk, K. Kang, *Energy Environ. Sci.* **2019**, *12*, 3144 – 3155.
[36] Y. Tsao, M. Lee, E. C. Miller, G. Gao, J. Park, S. Chen, T. Katsumata, H. Tran, L.-W. Wang, M. F. Toney, Y. Cui, Z. Bao, *Joule* **2019**, *3*, 872 – 884.
[37] G. Li, J. Sun, W. Hou, S. Jiang, Y. Huang, J. Geng, *Nat. Commun.* **2016**, *7*, 10601 – 10610.

[38] Y. S. Su, Y. Fu, T. Cochell, A. Manthiram, *Nat. Commun.* **2013**, *4*, 2985 – 2992.
[39] A. Bhargav, J. He, A. Gupta, A. Manthiram, *Joule* **2020**, *4*, 285 – 291.
[40] M. Shaibani, M. S. Mirshekarloo, R. Singh, C. D. Easton, M. C. D. Cooray, N. Eshraghi, T. Abendroth, S. Dorfler, H. Althues, S. Kaskel, A. F. Hollenkamp, M. R. Hill, M. Majumder, *Sci. Adv.* **2020**, *6*, eaay2757.
[41] C. Fang, J. Li, M. Zhang, Y. Zhang, F. Yang, J. Z. Lee, M. H. Lee, J. Alvarado, M. A. Schroeder, Y. Yang, B. Lu, N. Williams, M. Ceja, L. Yang, M. Cai, J. Gu, K. Xu, X. Wang, Y. S. Meng, *Nature* **2019**, *572*, 511 – 515.
[42] H. Li, *Joule* **2019**, *3*, 911 – 914.
[43] C. Niu, H. Lee, S. Chen, Q. Li, J. Du, W. Xu, J.-G. Zhang, M. S. Whittingham, J. Xiao, J. Liu, *Nat. Energy* **2019**, *4*, 551 – 559.